

Phase transformation and radiation resistance of B-site high entropy pyrochlores

Yuxin Li ^{a,1}, Yiming Lei ^{b,1}, Shuang Zhao ^a, Hao Xiao ^a, Haocheng Liu ^c, Yugang Wang ^a, Xixiu Luo ^b, Jie Zhang ^b, Jingyang Wang ^b, Rodney C. Ewing ^d, Chenxu Wang ^{a,*}

^a State Key Laboratory of Nuclear Physics and Technology, Center for Applied Physics and Technology, Peking University, Beijing 100871, China

^b Shenyang National Laboratory for Materials Science, Institute of Metal Research, Chinese Academy of Sciences, Shenyang 110016, China

^c State Power Investment Corporation Research Institute, Beijing 102209, China

^d Department of Geological Sciences, Stanford University, Stanford, CA 94305, USA



ARTICLE INFO

Keywords:

High entropy pyrochlore
Phase transformation
Radiation resistance
Fluorite structure

ABSTRACT

Two high entropy pyrochlores (HEPs), $\text{Gd}_2(\text{Ti}_{0.2}\text{Zr}_{0.2}\text{Sn}_{0.2}\text{Hf}_{0.2}\text{Ta}_{0.2})_2\text{O}_7$ and $\text{Gd}_2(\text{Ti}_{0.2}\text{Zr}_{0.2}\text{Sn}_{0.2}\text{Hf}_{0.2}\text{Nb}_{0.2})_2\text{O}_7$ have been synthesized and irradiated with 800 keV Kr^{2+} ions and examined by *in situ* transmission electron microscopy (TEM). The irradiation-induced order-to-disorder phase transformation from pyrochlore to the fluorite structure in these two HEPs and $\text{Gd}_2\text{Sn}_2\text{O}_7$ was observed by using selected area electron diffraction (SAED), high angle annular dark field scanning transmission electron microscopy (HAADF-STEM), and energy dispersive spectroscopy (EDS) mapping. The cation antisite defect (CAD) formation energy and the electron localization function (ELF) were calculated using density functional theory (DFT). Both the experimental results and calculated results suggest that the HEPs exhibit a higher resistance to phase transformation and amorphization than $\text{Gd}_2\text{Sn}_2\text{O}_7$.

Pyrochlore oxides with the chemical formula $\text{A}_2\text{B}_2\text{O}_7$ have attracted extensive attention in many fields, such as for thermal barrier coatings [1,2], fuel cells [3], catalysts [4], and as nuclear waste forms for actinides [5,6]. In pyrochlore, the A-site 16d (1/2,1/2,1/2) is usually occupied by lanthanides or actinides, coordinated with six 48f ($x,1/8,1/8$) oxygen atoms and two 8b (3/8,3/3/8) oxygen atoms. The B-site 16c (0,0,0) is usually a tetravalent transition metal or IVA group element, coordinated with six 48f oxygen atoms and adjacent to two 8a (1/8,1/8,1/8) oxygen vacancies [7]. Thus, the pyrochlore structure can be regarded as a derivative of the fluorite structure with A and B cation sites ordered and one-eighth vacancies in anion sites [8].

Previous studies have shown that the cations and the oxygen vacancies can become disordered and the structure transforms from pyrochlore to defect fluorite by thermal treatment [9], chemical substitution [9,10] or irradiation [11–13]. The irradiation triggers the formation of the CAD with the A- and B- cations displaced by the other. With the atomic evolution at the cation sites and the rearrangement of anions, the defect fluorite structure is formed. The formation of the CAD can help absorb point defects and maintain the stability of the structure

[14,15]. Therefore, the radiation tolerance of pyrochlore is related to the formation energy of the CAD, which strongly depends on the cation radius ratio r_A/r_B [16]. The smaller the cation radius ratio is, the lower the CAD formation energy is, the easier it is to form the fluorite structure, and the more irradiation-resistant it is [13,17,18]. In addition to the cation radius ratio, there are many other factors that also affect the radiation resistance of pyrochlores, among which the bond characteristic is often important [19]. It is generally believed that radiation tolerance can be promoted by increasing the ionic properties of the chemical bonds [20].

Recently, with the development of high entropy alloys [21], the concept of high-entropy was introduced into ceramics, and high entropy ceramics (HECs) have been proven to potentially possess excellent properties and wide applications [22–25]. Specifically, HEPs exhibit ultralow thermal conductivity [26], improved mechanical strength, and excellent electrochemical properties [27]. The phase transformation in ceramics is usually complex [28], and HECs exhibit better amorphization resistance than single-component ceramics [29]. However, the role of the high entropy effect on the irradiation-induced phase

* Corresponding author.

E-mail address: cwang@pku.edu.cn (C. Wang).

¹ These authors have contributed equally.

transformation and radiation resistance in HEPs is not clear yet. For example, Candice *et al.* showed that $(\text{Yb}_{0.2}\text{Tm}_{0.2}\text{Lu}_{0.2}\text{Ho}_{0.2}\text{Er}_{0.2})_2\text{Ti}_2\text{O}_7$ was comparable to that of single-component pyrochlores previously studied [30]. Liu *et al.* showed that the CAD is much easier to form in $\text{Gd}_2(\text{Ti}_{0.25}\text{Zr}_{0.25}\text{Sn}_{0.25}\text{Hf}_{0.25})_2\text{O}_7$ than $\text{Gd}_2\text{X}_2\text{O}_7$ ($\text{X} = \text{Ti}, \text{Zr}, \text{Sn}, \text{Hf}$), indicating that HEP could easily transfer to disordered fluorite structure and exhibit stronger radiation tolerance [31].

In this study, we designed and synthesized two high entropy oxides, $\text{Gd}_2(\text{Ti}_{0.2}\text{Zr}_{0.2}\text{Sn}_{0.2}\text{Hf}_{0.2}\text{Ta}_{0.2})_2\text{O}_7$ and $\text{Gd}_2(\text{Ti}_{0.2}\text{Zr}_{0.2}\text{Sn}_{0.2}\text{Hf}_{0.2}\text{Nb}_{0.2})_2\text{O}_7$, and a single-component pyrochlore $\text{Gd}_2\text{Sn}_2\text{O}_7$ for comparison *via* solid-state reaction [32,33], as shown in Fig. 1(a,b). The source ingredients were commercial Gd_2O_3 , SnO_2 , TiO_2 , ZrO_2 , Ta_2O_5 , Nb_2O_5 (99.99% purity) and HfO_2 powders (99.95% purity). To remove moisture, all raw oxide powders were dried at 1000 °C for 1 h, and then weighed in their respective stoichiometric ratio. The weighed powders were dissolved in anhydrous alcohol and mechanically ground for 24 h. Then, the slurry was dried at 80 °C for 12 h and subsequently passed through an 80-mesh sieve to obtain a homogeneous product. The powders of the samples were obtained after sintering at 1500 °C for 2 h. The XRD patterns in Fig. 1(c) illustrate that all three samples possess similar pyrochlore structures with high purity. Thereafter, the cylindrical green bodies of ceramics with a diameter of 8 mm and a thickness of 4 mm were fabricated *via* dry pressing, and then subjected to cold isostatic pressing at 260 MPa for 10 min. Finally, dense ceramic pellets were obtained after sintering at 1500 °C for 20 h without pressure.

Considering the strong influence of cation radius on radiation resistance [17,34], we designed the three materials with similar weighted cation radius ratios to exclude its influence, such that the role of the high entropy effect in the radiation resistance of these materials could be investigated. The cation radius ratio of $\text{Gd}_2\text{Sn}_2\text{O}_7$ is 1.53, and the average cation radius ratios of both high entropy oxides are 1.55 [35]. Therefore, the influence of the cation radius ratio can be excluded. The structure of $\text{Gd}_2\text{Sn}_2\text{O}_7$ with an 88-atom unit cell is shown in Fig. 1(a), where A-site is occupied by Gd^{3+} , and B-site is occupied by Sn^{4+} . Fig. 1(b) shows the structure of the HEPs, where A-site is occupied by Gd^{3+} ,

and B-site is occupied randomly by five elements ($\text{Ti}, \text{Zr}, \text{Sn}, \text{Hf}, \text{Ta}$ or Nb), each with an occupancy of 20%. The scanning electron microscope (SEM) images of the as-sintered materials demonstrate the uniformities in microstructure and microchemistry, as shown in Fig. S1.

To study the response of HEPs to irradiation, *in situ* irradiation experiments were performed at Xiamen University. The ion implanter is linked to a TEM, and the instrument can be switched between irradiation and observation modes. The samples were ground and polished manually, followed by ion thinning. Kr^{2+} with an energy of 800 keV were selected as incident ions at room temperature. The displacement per atom (dpa) was used as a parameter of irradiation doses to describe the irradiation damage to the materials, which is a function of fluence. The irradiation doses and the incident ion concentrations at an ion fluence of $2 \times 10^{15} \text{ cm}^{-2}$ are calculated using the SRIM code [36], as shown in Fig. 1(d). At the observation area under TEM, the thicknesses of samples estimated by electron energy loss spectrum (EELS) are shown in supplementary information and Fig. S2-S4, and the results show that the sample thickness is comparable.

Fig. 2 shows the SAED patterns of these three materials along [110] before and after irradiation. The damage level (dpa) and corresponding fluence are marked at the bottom of each pattern. For all these materials, the diffraction maxima ($2\bar{2}0$) and (002) attenuate compared to the patterns of the initial pyrochlore structures, as indicated by the white arrows in Fig. 2(a, b, g, h, m, n). This indicates that the anions disordered or weakly ordered, such that the intensities of diffraction maxima from the anions were undetectable by TEM techniques [7]. As the fluence increases, the diffraction maxima corresponding to cation ordering peaks (*i.e.*, $1\bar{1}1$, $1\bar{1}\bar{3}$) gradually weaken then disappear, indicated by the blue arrows in Fig. 2(b, c, h, i, n, o), suggesting the disorder of cations and the formation of defect fluorite structure induced by the accumulation of the cation antisite defects [7,37].

This phase transformation from pyrochlore to defect fluorite has been reported previously [7,14]. However, the detailed atomic structures and the chemical distribution of the defect fluorite transformed

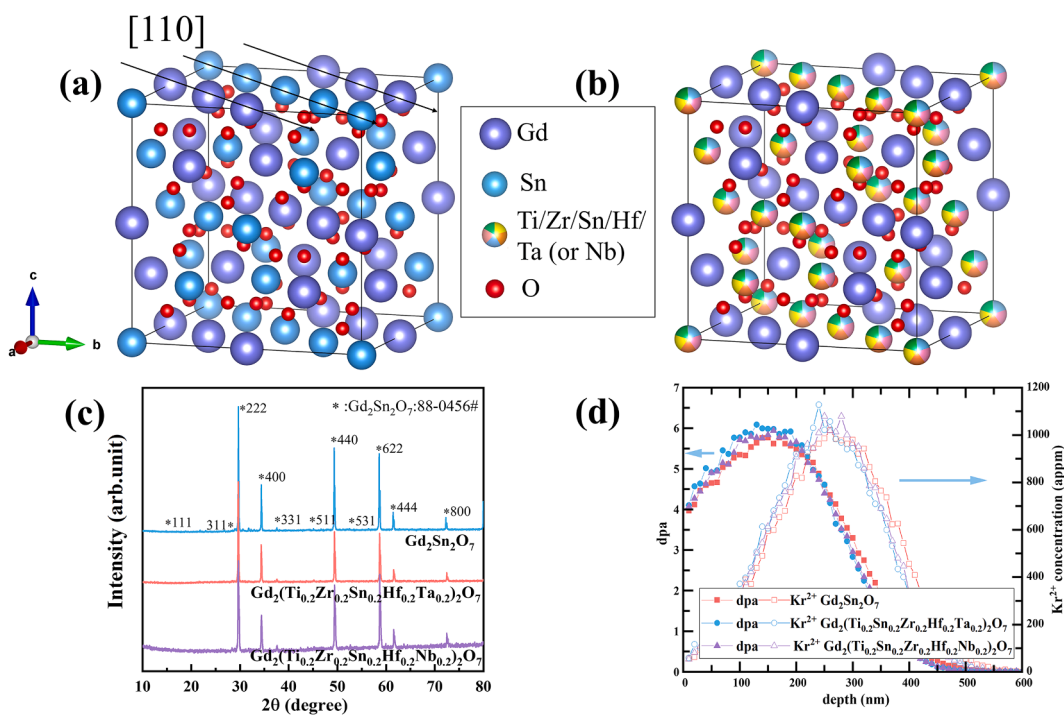


Fig. 1. Pyrochlore structure of (a) $\text{Gd}_2\text{Sn}_2\text{O}_7$ (b) $\text{Gd}_2(\text{Ti}_{0.2}\text{Zr}_{0.2}\text{Sn}_{0.2}\text{Hf}_{0.2}\text{Ta}_{0.2})_2\text{O}_7$ or $\text{Gd}_2(\text{Ti}_{0.2}\text{Zr}_{0.2}\text{Sn}_{0.2}\text{Hf}_{0.2}\text{Nb}_{0.2})_2\text{O}_7$, where the occupancies of cations ($\text{Ti}^{4+}, \text{Zr}^{4+}, \text{Sn}^{4+}, \text{Hf}^{4+}, \text{Ta}^{4+}$ or Nb^{4+}) at the B-site is 20%. (c) XRD patterns with characteristic peaks of pyrochlore. (d) The depth profiles of dpa and Kr^{2+} concentration calculated from SRIM at an ion fluence of $2 \times 10^{15} \text{ cm}^{-2}$. (For interpretation of the references to color in this figure legend, the reader is referred to the web version of this article.)

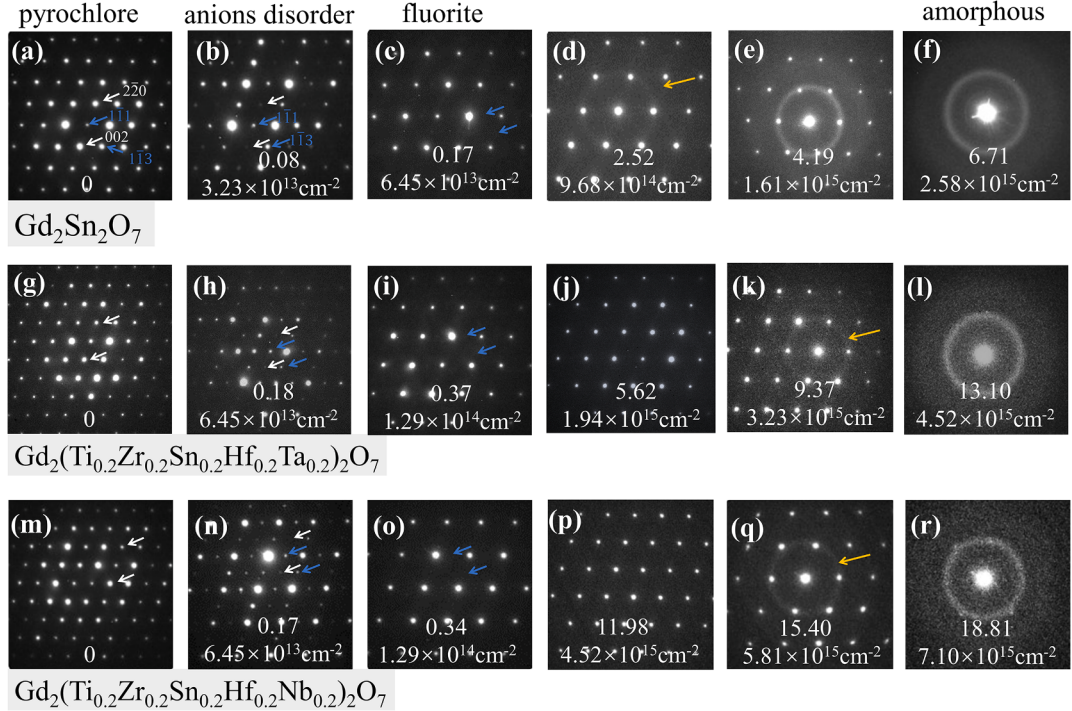


Fig. 2. SAED patterns along [110] from (a-f) $\text{Gd}_2\text{Sn}_2\text{O}_7$ (g-l) $\text{Gd}_2(\text{Ti}_{0.2}\text{Zr}_{0.2}\text{Sn}_{0.2}\text{Hf}_{0.2}\text{Ta}_{0.2})_2\text{O}_7$ (m-r) $\text{Gd}_2(\text{Ti}_{0.2}\text{Zr}_{0.2}\text{Sn}_{0.2}\text{Hf}_{0.2}\text{Nb}_{0.2})_2\text{O}_7$ irradiated by 800 keV Kr^{2+} at room temperature. The structures transform from pyrochlore to disorder fluorite to amorphization. The damage level (dpa) and fluence (cm^{-2}) are labeled at the bottom of each pattern. (For interpretation of the references to color in this figure legend, the reader is referred to the web version of this article.)

from the HEPs cannot be determined only based on the analysis of the SAED patterns. Therefore, we obtained HAADF-STEM and EDS mapping images of $\text{Gd}_2(\text{Ti}_{0.2}\text{Zr}_{0.2}\text{Sn}_{0.2}\text{Hf}_{0.2}\text{Nb}_{0.2})_2\text{O}_7$ along [110] by using spherical aberration-corrected transmission electron microscopy (SAC-TEM, Titan Cubed Themis G2 300). Fig. 3(a) shows the HAADF image of the original pyrochlore structure along [110] before irradiation, where the inset shows the intensity profile of the atomic columns indicated in the white box. In accordance with the relationship between intensity and the atomic number (Z) in the HAADF image, the contrast indicates the ordered arrangement of heavier cations at the A-site and lighter cations at the B-site [38]. Fig. 3(b-f) shows the overlapping result of the HAADF image and EDS mapping of Gd and B-site elements (Ti, Zr, Sn, Hf, and Nb), respectively. Most cations at the A- and B-sites are arranged orderly, with only a very small fraction of the atoms disordered.

Recent studies of the high entropy alloys and oxides suggest that chemical disorder can lead to the formation of mixed structures and atomic clustering [39–42].

The HAADF image obtained from the $\text{Gd}_2(\text{Ti}_{0.2}\text{Zr}_{0.2}\text{Sn}_{0.2}\text{Hf}_{0.2}\text{Nb}_{0.2})_2\text{O}_7$ sample after irradiation at about 0.3 dpa (1.3×10^{14} ions/ cm^2) is shown in Fig. 3(g). The contrast of each atomic column in this image becomes identical, which is confirmed by the intensity profile in the inset. This demonstrates that the cations have been sufficiently mixed, and the structure has completely transformed from an order pyrochlore to a disorder defect fluorite structure. The EDS mapping results of Gd and B-site elements (Ti, Zr, Sn, Hf, and Nb) in Fig. 3(h-l) demonstrate that the cations at A- and B-sites are randomly distributed and disordered at the cation sites.

With increasing irradiation fluence, amorphous rings appear in the

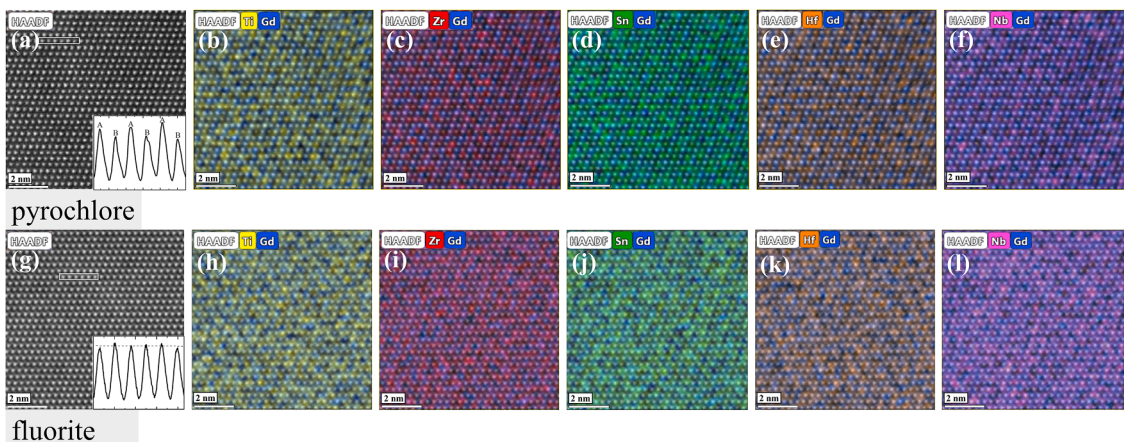


Fig. 3. HAADF images and the EDS mapping of $\text{Gd}_2(\text{Ti}_{0.2}\text{Zr}_{0.2}\text{Sn}_{0.2}\text{Hf}_{0.2}\text{Nb}_{0.2})_2\text{O}_7$ with the initial pyrochlore structure (a-f) before irradiation and the formed fluorite structure (g-l) after irradiation. The insets show the contrast profiles of the atomic column in the white box. (For interpretation of the references to color in this figure legend, the reader is referred to the web version of this article.)

SAED patterns of these three materials at the dose of 2.52 dpa (9.68×10^{14} ions/cm²), 9.37 dpa (3.23×10^{15} ions/cm²) and 15.4 dpa (5.81×10^{15} ions/cm²), respectively, as indicated by the yellow arrows in Fig. 2 (d, k, q). This indicates the atomic disordering of the fluorite structure. Fig. 2(j, p) show that the HEPs maintain the fluorite structure at a dose of 5.62 (1.94×10^{15} ions/cm²) and 11.98 dpa (4.52×10^{15} ions/cm²), which is higher than 2.52 dpa (9.68×10^{14} ions/cm²), demonstrating their stronger ability to maintain fluorite structure under irradiation. As the dose continued to increase, the fluorite structures are completely amorphized, as shown in Fig. 2(f, l, r). The threshold doses for amorphization in these three samples are about 6.71 dpa (2.58×10^{15} ions/cm²), 13.10 dpa (4.52×10^{15} ions/cm²) and 18.81 dpa (7.10×10^{15} ions/cm²), respectively, as shown in Table 1. The difference of the threshold doses indicates that the two HEPs, in particular Gd₂(Ti_{0.2}Zr_{0.2}Sn_{0.2}Hf_{0.2}Nb_{0.2})₂O₇, are more resistant to the irradiation-induced phase transformation and amorphization than Gd₂Sn₂O₇.

The reasons for the different radiation resistance of three materials were analyzed by first-principles calculation. Defect formation energies are used to compare the single compound pyrochlore and HEPs, and the bonding characteristics calculated by ELF are further analysis between HEPs [43,44]. The calculations were based on DFT and implemented in the Vienna Ab Initio Simulation Package (VASP) [45]. The Perdew Burke Ernzerhof (PBE) [46] functional under the electronic exchange-correlation function of generalized gradient approximation (GGA) [47] was used. The kinetic cutoff energy was set to be 500 eV and a $2 \times 2 \times 2$ k-point was taken. A unit cell of 88 atoms with HEP structure was generated by a special quasi-random structure (SQS) approach [48, 49] and 10 structures were constructed for both HEPs.

There are five types of CAD for two HEPs due to the random distribution of five elements at the B site. The 20 configurations that were taken for each type of CAD (a total of 100 defects for each HEP), because the CAD formation energies differ in various local chemical environments. Table 2 shows the results of the CAD defect formation energy and other information on the relaxed initial pyrochlore structures, which are in good agreement with the calculated results [31,50,51]. The cation structure distortion is the average displacement distance of all the cations from the ideal lattice position in 10 structures.

The defect formation energies of the two HEPs ($1.19 \text{ eV} \pm 0.17$ and $1.35 \text{ eV} \pm 0.25$) are significantly lower than that of Gd₂Sn₂O₇ (2.96 eV). This result indicates that the fluorite structure for two HEPs would be more preferred than Gd₂Sn₂O₇. However, the CAD forming energies of the two HEPs are similar within the error range because they highly depend on the local chemical environment. Therefore, the CAD formation energies are not sufficient to evaluate radiation resistance among the two HEPs, and more analysis such as bonding characteristics is needed due to the existence of different elements in these two HEPs.

The role of chemical bonds has been studied in pyrochlores,

Table 1

The fluence (ions/cm²) and damage level (dpa) as the fluorite phase formation, amorphous diffraction ring appearance, and amorphous phase formation occur in these materials, respectively.

Sample	Fluorite phase formation	Diffraction ring appearance	Amorphous phase formation
Gd ₂ Sn ₂ O ₇	3.23×10^{13} ions/cm ²	9.68×10^{14} ions/cm ²	2.58×10^{15} ions/cm ²
Gd ₂ (Ti _{0.2} Zr _{0.2} Sn _{0.2} Hf _{0.2} Ta _{0.2}) ₂ O ₇	6.45×10^{13} ions/cm ²	3.23×10^{15} ions/cm ²	4.52×10^{15} ions/cm ²
Gd ₂ (Ti _{0.2} Zr _{0.2} Sn _{0.2} Hf _{0.2} Nb _{0.2}) ₂ O ₇	6.45×10^{13} ions/cm ²	5.81×10^{15} ions/cm ²	7.10×10^{15} ions/cm ²

Table 2

Structural parameters and CAD formation energy of Gd₂Sn₂O₇, Gd₂(Ti_{0.2}Zr_{0.2}Sn_{0.2}Hf_{0.2}Ta_{0.2})₂O₇ and Gd₂(Ti_{0.2}Zr_{0.2}Sn_{0.2}Hf_{0.2}Nb_{0.2})₂O₇.

Sample	r _A /r _B	Unit cell parameter (Å)	Cation structure distortion (Å)	CAD formation energy (eV)
Gd ₂ Sn ₂ O ₇	1.53	10.55	/	2.96
Gd ₂ (Ti _{0.2} Zr _{0.2} Sn _{0.2} Hf _{0.2} Ta _{0.2}) ₂ O ₇	1.55	10.48	0.084	1.19 ± 0.17
Gd ₂ (Ti _{0.2} Zr _{0.2} Sn _{0.2} Hf _{0.2} Nb _{0.2}) ₂ O ₇	1.55	10.47	0.079	1.35 ± 0.25

indicating that of the two possible cation sites, the B-site cation appears to play the major role in bonding [19,20]. The covalent networks are not conducive to atomic rearrangement and leads to more severe damage, while higher ionicity leads to higher radiation resistance and a better ability to maintain the disordered structure [52]. For complex oxides, the type of interatomic force defines how atoms interact and rearrange within a material. Therefore, the amorphous resistance induced by ion irradiation is strongly influenced by the chemical bond characteristics and is sensitive to the elements [52,53]. In this work, the ELF were used to explore the electron distribution and bond characteristic in these three pyrochlores [43], as shown in Fig. 4. The data was analyzed by VESTA software [54].

To visually analyze the electrons between each cation and O, we cut out the 2D {110} lattice planes, where logarithmic contours are used and the value ranges from 0 to 0.65 (e/Bohr³). It can be seen that the electrons around Sn are delocalized and a lot of electrons are involved in bonding with O in Fig. 4(a,b), indicating that the $\langle \text{Sn}—\text{O} \rangle$ bond is very covalent. For the B-site cations of Gd₂(Ti_{0.2}Zr_{0.2}Sn_{0.2}Hf_{0.2}Nb_{0.2})₂O₇, the electrons are more localized around Zr, and delocalized around Sn, Ti and Hf, which is the same with Gd₂(Ti_{0.2}Zr_{0.2}Sn_{0.2}Hf_{0.2}Ta_{0.2})₂O₇, as shown in Fig. 4(c, d, e, f). However, it should be noted that the electrons around Nb are much more localized than that around Ta. Besides, there are many fewer electrons around Nb involved in bonding with O than Ta. This indicates that the $\langle \text{Nb}—\text{O} \rangle$ bond is much more ionic than the

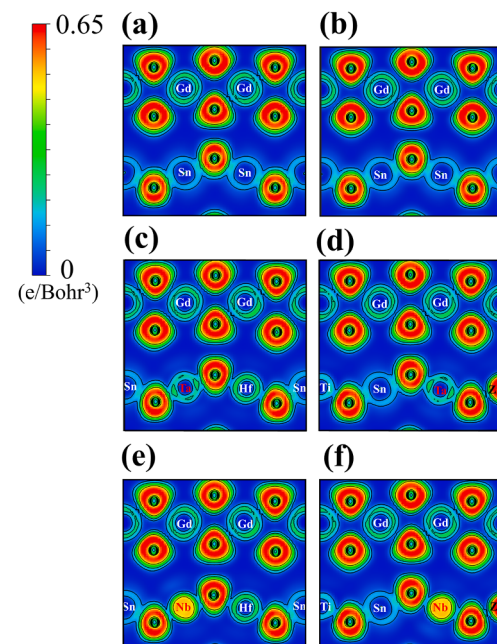


Fig. 4. ELF in {110} planes of (a,b) Gd₂Sn₂O₇, (c,d) Gd₂(Ti_{0.2}Zr_{0.2}Sn_{0.2}Hf_{0.2}Ta_{0.2})₂O₇, (e,f) Gd₂(Ti_{0.2}Zr_{0.2}Sn_{0.2}Hf_{0.2}Nb_{0.2})₂O₇. (For interpretation of the references to color in this figure legend, the reader is referred to the web version of this article.)

$\langle \text{Ta}—\text{O} \rangle$ bond. Therefore, $\text{Gd}_2(\text{Ti}_{0.2}\text{Zr}_{0.2}\text{Sn}_{0.2}\text{Hf}_{0.2}\text{Nb}_{0.2})_2\text{O}_7$ is more resistant to amorphization induced by ion irradiation and the fluorite structure of $\text{Gd}_2(\text{Ti}_{0.2}\text{Zr}_{0.2}\text{Sn}_{0.2}\text{Hf}_{0.2}\text{Nb}_{0.2})_2\text{O}_7$ is more stable when the atoms are displaced and rearranged under irradiation.

In summary, we designed and synthesized a single component pyrochlore ($\text{Gd}_2\text{Sn}_2\text{O}_7$) and two HEPs ($\text{Gd}_2(\text{Ti}_{0.2}\text{Zr}_{0.2}\text{Sn}_{0.2}\text{Hf}_{0.2}\text{Ta}_{0.2})_2\text{O}_7$ and $\text{Gd}_2(\text{Ti}_{0.2}\text{Zr}_{0.2}\text{Sn}_{0.2}\text{Hf}_{0.2}\text{Nb}_{0.2})_2\text{O}_7$) with similar cation radius ratios. *In situ* irradiation experiments were completed on these samples, and the order-to-disorder phase transformation from pyrochlore to defect fluorite and the subsequent amorphization process were observed. The distribution of cations in HEPs was revealed at the atomic scale. The cations are alternately ordered in the pyrochlore structure and randomly disordered in the fluorite structure. The difference in the threshold dose for amorphization in these materials indicates that the radiation resistance of $\text{Gd}_2(\text{Ti}_{0.2}\text{Zr}_{0.2}\text{Sn}_{0.2}\text{Hf}_{0.2}\text{Nb}_{0.2})_2\text{O}_7$ is better than $\text{Gd}_2(\text{Ti}_{0.2}\text{Zr}_{0.2}\text{Sn}_{0.2}\text{Hf}_{0.2}\text{Ta}_{0.2})_2\text{O}_7$ and much better than $\text{Gd}_2\text{Sn}_2\text{O}_7$. The calculations at the atomic level by DFT show that the CAD formation energies of HEPs are much smaller than that of $\text{Gd}_2\text{Sn}_2\text{O}_7$, yet this may not be distinguished among HEPs. Further bonding characteristic analysis shows that the bonds in $\text{Gd}_2(\text{Ti}_{0.2}\text{Zr}_{0.2}\text{Sn}_{0.2}\text{Hf}_{0.2}\text{Nb}_{0.2})_2\text{O}_7$ are more ionic than that in $\text{Gd}_2(\text{Ti}_{0.2}\text{Zr}_{0.2}\text{Sn}_{0.2}\text{Hf}_{0.2}\text{Ta}_{0.2})_2\text{O}_7$. The effects of chemical disorder and bonding characteristics both influence the radiation resistance of HEPs.

Declaration of Competing Interest

The authors declare that they have no competing interests.

Acknowledgments

The authors thank the Multiion Beam *In Situ* Analysis Laboratory of Xiamen University for providing irradiation experiments and Jinchi Huang, Zhehui Zhou, Yan Liu, and Pengfei Ma for their assistance with the *in situ* irradiation experiments. We also acknowledge the Electron Microscopy Laboratory of Peking University, China for the use of Cs corrected Titan Cubed Themis G2 200 transmission electron microscopy and Beijing Super Cloud Computing Center for the first-principle calculations. This work was supported by the National Natural Science Foundation of China (Grant No. 12275009, 12192280, and 11935004), and the National Magnetic Confinement Fusion Energy Research Project 2021YFE031100.

Supplementary materials

Supplementary material associated with this article can be found, in the online version, at doi:10.1016/j.scriptamat.2023.115367.

References

- [1] D.R. Clarke, M. Oechsner, N.P. Padture, Thermal-barrier coatings for more efficient gas-turbine engines, *MRS Bull.* 37 (2012) 891–898.
- [2] X.Q. Cao, R. Vassen, F. Tietz, D. Stoever, New double-ceramic-layer thermal barrier coatings based on zirconia–rare earth composite oxides, *J. Eur. Ceram. Soc.* 26 (2006) 247–251.
- [3] F. Zhong, S. Yang, C. Chen, H. Fang, K. Chen, C. Zhou, L. Lin, Y. Luo, C. Au, L. Jiang, Defect-induced pyrochlore $\text{Pr}_2\text{Zr}_2\text{O}_7$ cathode rich in oxygen vacancies for direct ammonia solid oxide fuel cells, *J. Power Sources* 520 (2022), 230847.
- [4] S.H. Oh, R. Black, E. Pomerantseva, J.H. Lee, L.F. Nazar, Synthesis of a metallic mesoporous pyrochlore as a catalyst for lithium– O_2 batteries, *Nat. Chem.* 4 (2012) 1004–1010.
- [5] X. Shu, L. Fan, Y. Xie, W. Zhu, S. Pan, Y. Ding, F. Chi, Y. Wu, X. Lu, Alpha-particle irradiation effects on uranium-bearing $\text{Gd}_2\text{Zr}_2\text{O}_7$ ceramics for nuclear waste forms, *J. Eur. Ceram. Soc.* 37 (2017) 779–785.
- [6] R.C. Ewing, W.J. Weber, J. Lian, Nuclear waste disposal—Pyrochlore ($\text{A}_2\text{B}_2\text{O}_7$): nuclear waste form for the immobilization of plutonium and “minor” actinides, *J. Appl. Phys.* 95 (2004) 5949–5971.
- [7] J. Lian, L. Wang, J. Chen, K. Sun, R.C. Ewing, J.M. Farmer, L.A. Boatner, The order-disorder transition in ion-irradiated pyrochlore, *Acta Mater.* 51 (2003) 1493–1502.
- [8] M.A. Subramanian, G. Aravamudan, G.V. Subba Rao, Oxide pyrochlores — A review, *Prog. Solid State Chem.* 15 (1983) 55–143.
- [9] B.J. Wuensch, K.W. Eberman, Order-disorder phenomena in $\text{A}_2\text{B}_2\text{O}_7$ pyrochlore oxides, *JOM* 52 (2000) 19–21.
- [10] A.F. Fuentes, S.M. Montemayor, M. Maczka, M. Lang, R.C. Ewing, U. Amador, A critical review of existing criteria for the prediction of pyrochlore formation and stability, *Inorg. Chem.* 57 (2018) 12093–12105.
- [11] J. Lian, L.M. Wang, S.X. Wang, J. Chen, L.A. Boatner, R.C. Ewing, Nanoscale manipulation of pyrochlore: new nanocomposite ionic conductors, *Phys. Rev. Lett.* 87 (2001) 145901.
- [12] S.X. Wang, L.M. Wang, R.C. Ewing, K.V. Govindan Kutty, Ion irradiation of rare-earth- and yttrium-titanate-pyrochlores, *Nucl. Instruments Methods Phys. Res. Sect. B Beam Interact. Mater. Atoms* 169 (2000) 135–140.
- [13] J. Lian, X.T. Zu, K.V.G. Kutty, J. Chen, L.M. Wang, R.C. Ewing, Ion-irradiation-induced amorphization of $\text{La}_2\text{Zr}_2\text{O}_7$ pyrochlore, *Phys. Rev. B* 66 (2002) 541081–541085.
- [14] J. Lian, J. Chen, L.M. Wang, R.C. Ewing, J.M. Farmer, L.A. Boatner, K.B. Helean, Radiation-induced amorphization of rare-earth titanate pyrochlores, *Phys. Rev. B* 68 (2003), 134107.
- [15] L. Minervini, R.W. Grimes, K.E. Sickafus, Disorder in pyrochlore oxides, *J. Am. Ceram. Soc.* 83 (2000) 1873–1878.
- [16] K.E. Sickafus, L. Minervini, R.W. Grimes, J.A. Valdez, M. Ishimaru, F. Li, K. J. McLellan, T. Hartmann, Radiation tolerance of complex oxides, *Science* 289 (2000) 748–751.
- [17] C.L. Tracy, J. Shamblin, S. Park, F. Zhang, C. Trautmann, M. Lang, R.C. Ewing, Role of composition, bond covalency, and short-range order in the disordering of stannate pyrochlores by swift heavy ion irradiation, *Phys. Rev. B* 94 (2016), 064102.
- [18] R.W.G. Sickafus, J.A. Valdez, A. Cleave, M. Tang, M. Ishimaru, S.M. Corish, C. R. Stanek, B.P. Uberuaga, Radiation-induced amorphization resistance and radiation tolerance in structurally related oxides, *Nat. Mater.* 6 (2007) 217–223.
- [19] Z.J. Chen, H.Y. Xiao, X.T. Zu, L.M. Wang, F. Gao, J. Lian, R.C. Ewing, Structural and bonding properties of stannate pyrochlores: a density functional theory investigation, *Comput. Mater. Sci.* 42 (2008) 653–658.
- [20] G.R. Lumpkin, M. Pruneda, S. Rios, K.L. Smith, K. Trachenko, K.R. Whittle, N. J. Zaluzec, Nature of the chemical bond and prediction of radiation tolerance in pyrochlore and defect fluorite compounds, *J. Solid State Chem.* 180 (2007) 1512–1518.
- [21] D.B. Miracle, O.N. Senkov, A critical review of high entropy alloys and related concepts, *Acta Mater.* 122 (2017) 448–511.
- [22] H. Xiang, Y. Xing, F. zhi Dai, H. Wang, L. Su, L. Miao, G. Zhang, Y. Wang, X. Qi, L. Yao, H. Wang, B. Zhao, J. Li, Y. Zhou, High-entropy ceramics: present status, challenges, and a look forward, *J. Adv. Ceram.* 10 (2021) 385–441.
- [23] X. Ren, T. Zhan, J. Zhang, J. Wang, Equiatomic quaternary $(\text{Y}_{1/4}\text{Ho}_{1/4}\text{Er}_{1/4}\text{Y}_{1/4})_2\text{SiO}_5$ silicate: a perspective multifunctional thermal and environmental barrier coating material, *Scr. Mater.* 168 (2019) 47–50.
- [24] Y. Zhang, W.M. Guo, Z. Bin Jiang, Q.Y. Zhu, S.K. Sun, Y. You, K. Plucknett, H. T. Lin, Dense high-entropy boride ceramics with ultra-high hardness, *Scr. Mater.* 164 (2019) 135–139.
- [25] J. Zhu, J. Xu, P. Zhang, X. Meng, S. Cao, J. Wu, M. Wei, Y. Shi, M.J. Reece, F. Gao, *Scr. Mater.* 200 (2021), 113912.
- [26] Z. Zhao, H. Xiang, F.Z. Dai, Z. Peng, Y. Zhou, $(\text{La}_{0.2}\text{Ce}_{0.2}\text{Nd}_{0.2}\text{Sm}_{0.2}\text{Eu}_{0.2})_2\text{Zr}_2\text{O}_7$: a novel high-entropy ceramic with low thermal conductivity and sluggish grain growth rate, *J. Mater. Sci. Technol.* 35 (2019) 2647–2651.
- [27] K. Ren, Q. Wang, G. Shao, X. Zhao, Y. Wang, Multicomponent high-entropy zirconates with comprehensive properties for advanced thermal barrier coating, *Scr. Mater.* 178 (2020) 382–386.
- [28] C. Wang, T. Yang, C.L. Tracy, C. Lu, H. Zhang, Y.-J. Hu, L. Wang, L. Qi, L. Gu, Q. Huang, J. Zhang, J. Wang, J. Xue, R.C. Ewing, Y. Wang, Disorder in $\text{M}_{n+1}\text{AX}_n$ phases at the atomic scale, *Nat. Commun.* 10 (2019) 622.
- [29] S. Zhao, L. Chen, H. Xiao, J. Huang, Y. Li, Y. Qian, T. Zheng, Y. Li, L. Cao, H. Zhang, H. Liu, Y. Wang, Q. Huang, C. Wang, Phase transformation and amorphization resistance in high-entropy MAX phase M_2SnC ($\text{M} = \text{Ti}, \text{V}, \text{Nb}, \text{Zr}, \text{Hf}$) under *in-situ* ion irradiation, *Acta Mater.* 238 (2022), 118222.
- [30] C. Kinsler-Fedor, L. Nickols, C. Nelson, Z. Qi, Q. Huang, D. Mandrus, Y. Zhang, W. J. Weber, V. Keppens, Effects of Au^{2+} irradiation induced damage in a high-entropy pyrochlore oxide single crystal, *Scr. Mater.* 220 (2022), 114916.
- [31] C. Liu, Q. Peng, T. Shi, F. Gao, Y. Li, Physical properties and radiation tolerance of high-entropy pyrochlores $\text{Gd}_2(\text{Ti}_{0.25}\text{Zr}_{0.25}\text{Sn}_{0.25}\text{Hf}_{0.25})_2\text{O}_7$ and individual pyrochlores $\text{Gd}_2\text{X}_2\text{O}_7$ ($\text{X} = \text{Ti}, \text{Zr}, \text{Sn}, \text{Hf}$) from first principles calculations, *Scr. Mater.* 220 (2022), 114898.
- [32] X. Lv, J. Cui, J. Zhang, J. Wang, Phase composition and property evolution of $(\text{Yb}_{1-x}\text{Ho}_x)_2\text{Si}_2\text{O}_7$ solid solution as environmental/thermal barrier coating candidates, *J. Eur. Ceram. Soc.* 42 (2022) 4377–4387.
- [33] W.P. Hu, G.H. Zhang, Y.M. Lei, L.C. Sun, J. Zhang, and J.Y. Wang, Mechanical and thermal properties of $\delta\text{-RE}_4\text{HF}_3\text{O}_12$ ($\text{RE}=\text{Yb}, \text{Lu}$), *Inter. J. Applied Ceram. Techn.* (2023) in print.
- [34] B.D. Begg, N.J. Hess, D.E. McCready, S. Thevuthasan, W.J. Weber, Heavy-ion irradiation effects in $\text{Gd}_2(\text{Ti}_{2-x}\text{Zr}_x)\text{O}_7$ pyrochlores, *J. Nucl. Mater.* 289 (2001) 188–193.
- [35] R.D. Shannon, Revised effective ionic radii and systematic studies of interatomic distances in halides and chalcogenides, *Acta Cryst. Sect. A* 32 (1976) 751–767.
- [36] J.F. Ziegler, J.P. Biersack, U. Littmark, *The Stopping and Ranges of Ions in Solids*, Pergamon Press, New York, 1985. <http://www.srim.org/>.
- [37] J. Lian, L.M. Wang, R.G. Haire, K.B. Helean, R.C. Ewing, Ion beam irradiation in $\text{La}_2\text{Zr}_2\text{O}_7\text{-Ce}_2\text{Zr}_2\text{O}_7$ pyrochlore, *Nucl. Instruments Methods Phys. Res. Sect. B Beam Interact. Mater. Atoms* 218 (2004) 236–243.

- [38] R. Sachan, E. Zarkadoula, M. Lang, C. Trautmann, Y. Zhang, M.F. Chisholm, W. J. Weber, Insights on dramatic radial fluctuations in track formation by energetic ions, *Sci. Rep.* 6 (2016) 2–8.
- [39] X. Chen, Q. Wang, Z. Cheng, M. Zhu, H. Zhou, P. Jiang, L. Zhou, Q. Xue, F. Yuan, J. Zhu, X. Wu, E. Ma, Direct observation of chemical short-range order in a medium-entropy alloy, *Nature* 592 (2021) 712–716.
- [40] B. Jiang, C.A. Bridges, R.R. Unocic, K.C. Pitike, V.R. Cooper, Y. Zhang, D.-Y. Lin, K. Page, Probing the local site disorder and distortion in pyrochlore high-entropy oxides, *J. Am. Chem. Soc.* 143 (2021) 4193–4204.
- [41] R. Zhang, S. Zhao, J. Ding, Y. Chong, T. Jia, C. Ophus, M. Asta, R.O. Ritchie, A. M. Minor, Short-range order and its impact on the CrCoNi medium-entropy alloy, *Nature* 581 (2020) 283–287.
- [42] D.L. Drey, E.C. O’Quinn, T. Subramani, K. Lilova, G. Baldinozzi, I.M. Gussev, A. F. Fuentes, J.C. Neufeind, M. Everett, D. Sprouster, A. Navrotsky, R.C. Ewing, M. Lang, Disorder in $\text{Ho}_{2\text{Tl}_2-\text{xZr}_x}\text{O}_7$: pyrochlore to defect fluorite solid solution series, *RSC Adv.* 10 (2020) 34632–34650.
- [43] A.D. Becke, K.E. Edgecombe, A simple measure of electron localization in atomic and molecular systems, *J. Chem. Phys.* 92 (1990) 5397.
- [44] C.G. Liu, Y.H. Li, Y.D. Li, L.Y. Dong, J. Wen, D.Y. Yang, Q.L. Wei, P. Yang, First principle calculation of helium in $\text{La}_2\text{Zr}_2\text{O}_7$: effects on structural, electronic properties and radiation tolerance, *J. Nucl. Mater.* 500 (2018) 72–80.
- [45] G. Kresse, J. Furthmüller, Efficient iterative schemes for ab initio total-energy calculations using a plane-wave basis set, *Phys. Rev. B* 54 (1996) 11169.
- [46] D.J. Chadi, Special points for Brillouin-zone integrations, *Phys. Rev. B* 16 (1977) 1746.
- [47] P.E. Blöchl, Projector augmented-wave method, *Phys. Rev. B* 50 (1994) 17953.
- [48] A. Zunger, S.H. Wei, L.G. Ferreira, J.E. Bernard, Special quasirandom structures, *Phys. Rev. Lett.* 65 (1990) 353.
- [49] S.H. Wei, L.G. Ferreira, J.E. Bernard, A. Zunger, Electronic properties of random alloys: special quasirandom structures, *Phys. Rev. B* 42 (1990) 9622.
- [50] Y. Li, P.M. Kowalski, G. Beridze, A.R. Birnie, S. Finkeldei, D. Bosbach, Defect formation energies in $\text{A}_2\text{B}_2\text{O}_7$ pyrochlores, *Scr. Mater.* 107 (2015) 18–21.
- [51] Y.H. Wang, Y.H. Li, C.G. Liu, X. Liu, First-principles study of plutonium and cerium solubility in $\text{Gd}_2\text{Sn}_2\text{O}_7$ pyrochlore, *Nucl. Instruments Methods Phys. Res. Sect. B Beam Interact. Mater. Atoms* 436 (2018) 211–216.
- [52] K. Trachenko, Understanding resistance to amorphization by radiation damage, *J. Phys. Condens. Matter* 16 (2004) R1491–R1515.
- [53] W.R. Panero, L. Stixrude, R.C. Ewing, First-principles calculation of defect-formation energies in the $\text{Y}_2(\text{Ti},\text{Sn},\text{Zr})_2\text{O}_7$ pyrochlore, *Phys. Rev. B* 70 (2004) 1–11.
- [54] K. Momma, F. Izumi, VESTA3 for three-dimensional visualization of crystal, volumetric and morphology data, *J. Appl. Cryst.* 44 (2011) 1272–1276.